Proton Transfers Induced by Lead(II) in a Uracil Nucleobase: A Study Based on Quantum Chemistry Calculations

C. Gutlé, J.-Y. Salpin, T. Cartailler, J. Tortajada, and M.-P. Gaigeot*

Université d'Evry val d'Essonne, Laboratoire Analyse et Modélisation pour la Biologie et l'Environnement, LAMBE UMR-8587, Rue Père A. Jarland, F-91025 Evry, France

Received: April 6, 2006; In Final Form: August 2, 2006

Within the context of metal biotoxicity, electrospray ionization mass spectrometry experiments (ESIMS) have recently been performed by us on the pyrimidine nucleobases (B) uracil and thymine complexed with lead(II) [*Int. J. Mass. Spectrom.* **2005**, *243*, 279]. Among the ions detected, $[Pb(B)-H]^+$ complexes, where the base has been deprotonated, have been identified as producing intense signals. In the same study, quantum calculations based on density functional theory (DFT) have assessed the complexation sites and energies of $[Pb(B)-H]^+$ ions. The present DFT investigations aim at giving an understanding on the energetics and mechanisms associated with uracil's loss of a proton. We specifically assess and quantify the role of lead binding in this process. For that purpose, intra- and intermolecular proton transfers have been considered. We have found that uracil (U) 1,3-tautomerization can be exergonic when uracil is complexed with Pb^{2+}, in opposition to the situation without lead. The corresponding intramolecular processes were nonetheless found to occur at geological time scales. In contrast, the addition of a second body to $[Pb(U)]^{2+}$ complexes, namely OH^- or H_2O (as found in the initial water droplet of ESIMS experiments), gives exergonic and fast uracil 1,3-proton transfers. Finally, we have shown that intermolecular proton transfers in uracil−H_2O, uracil−OH^-, or uracil−uracil complexes are able to explain the experimentally detected $[Pb(U)-H]^+$ ions.

1. Introduction

The binding of metal ions to biomolecules is recognized as a fundamental aspect to activate or deactivate their chemical and biological activities. As a few examples, metals are able to deeply modify three-dimensional structures,[1] they play a role in chiral molecular recognition,[2] and they are known to induce chemical reactions such as intra- or intermolecular electron- or proton-transfer processes and deprotonation mechanisms.[3−6] The present study is related to these last two points, as it focuses on the role of a heavy metal, lead, as a promoter of intramolecular proton transfer and as a deprotonation agent in nucleic acids.

In the past few years, our group has undertaken investigations of metal binding to building blocks of nucleic acids, peptides, and sugars,[7−12] with a combination of either positive-ion electrospray ionization (ESI) or fast atom bombardment (FAB) mass spectrometry (MS) experiments and DFT (density functional theory) quantum chemistry calculations. Our goal is to obtain intrinsic information about the gas-phase reactivity between metals and these building blocks in a "bottom-up" approach (i.e., in a strategy based on the gradual increase of the size and complexity of the building blocks). In this context, we have started our investigations on metal−nucleic acids binding, with nucleobases such as thymine (DNA nucleobase) and uracil (RNA nucleobase) complexed with lead. Our previous ESIMS and quantum calculations on that subject are reported in ref 12. See also ref 13 for a review on the interactions of lead(II) with nucleotides and their constituents.

Deprotonation of biomolecules induced by metal chelation can be especially observed in the gas phase, as shown by us or by other groups with ESIMS experiments.[7−9,12,14−19] A recurrent question about these experiments is whether deprotonation occurs in the aqueous phase (i.e., within the water droplet in which the metal−biomolecule complex is initially trapped) or in the gas phase after all water molecules have evaporated. Some studies do support the assumption that the gas-phase species obtained in mass spectrometry reflect the solution species.[20] We propose here to give more insights on this question in the specific case of the lead−uracil complexes.

As an illustration of metal-induced deprotonation, the positive-ion ESIMS mass spectrum of an aqueous mixture of lead nitrate ($Pb(NO_3)_2$) and uracil with a cone voltage set to 100 V is presented in Figure 2. The experimental conditions are identical to those given in ref 12 where this spectrum was not included. We find three types of ionic complexes.

The first series corresponds to singly charged species where a deprotonated uracil (U) is complexed with lead, water, and nitrates. This is illustrated by the peaks located at $m/z = 319$, 337, 355, and 382, corresponding to $[Pb(U)-H]^+$, $[Pb(U)-H(H_2O)_{n=1,2}]^+$, and $[Pb(U)-H(HNO_3)]^+$, respectively. The second series corresponds to heavier singly charged leaded cations ($[Pb(U_m)-H]^+$) that exhibit clusters of uracil molecules among which one has lost one proton. See peaks related to $[Pb(U_2)-H]^+$, $[Pb(U_2)-H(H_2O)]^+$, $[Pb(U_2)-H(HNO_3)]^+$, $[Pb(U_3)-H]^+$, $[Pb(U_3)-H(HNO_3)]^+$, and $[Pb(U_4)-H]^+$ at $m/z = 431$, 449, 494, 543, 606, and 655, respectively.

Doubly charged ions $[Pb(U_n)]^{2+}$ are not visible in the experimental ESIMS spectrum, although they are known to produce peaks of low intensities under gentle ionization conditions.[12] Their absence in our mass spectrum most likely comes from the superposition of $[Pb(U_n)]^{2+}$ peaks with those of more abundant singly charged species. For instance, $[Pb(U_7)]^{2+}$ and $[Pb(U_2)(HNO_3)]^+$ are expected at $m/z = 496$ and

* Corresponding author. E-mail: gaigeot@ccr.jussieu.fr. Permanent address: LPTMC, Université Pierre et Marie Curie-Paris6, UMR-CNRS 7600, 4 Place Jussieu, Case Courrier 121, F-75052 Paris, France.

10.1021/jp0621528 CCC: $33.50
Published on Web 09/26/2006

		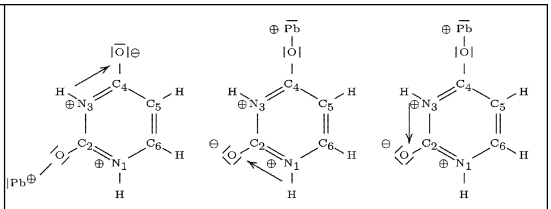 $N_3 \rightarrow O_8$ (U_2)	$N_1 \rightarrow O_7$ (U_1)	$N_3 \rightarrow O_7$ (U_4)
without lead	ϵ_R^{ZPE} (a.u.)	-414.730	-414.730	-414.730
	ϵ_P^{ZPE} (a.u.)	-414.711	-414.713	-414.700
	ΔG (kcal.mol^{-1})	+12	+11	+20
	$\Delta G^{\ddagger}$ (kcal.mol^{-1})	35	36	41
	ν (cm^{-1})	1854	1848	1858
with Pb^{2+}	ϵ_R^{ZPE} (a.u.)	-417.533	-417.551	-417.551
	ϵ_P^{ZPE} (a.u.)	-417.566	-417.544	-417.566
	ΔG (kcal.mol^{-1})	-20	+5	-8
	$\Delta G^{\ddagger}$ (kcal.mol^{-1})	29	42	36
	ν (cm^{-1})	1836	1872	1870
with $Pb(H_2O)^{2+}$	ϵ_R^{ZPE} (a.u.)	-493.994	-494.011	-494.011
	ϵ_P^{ZPE} (a.u.)	-494.024	-494.002	-494.025
	ΔG (kcal.mol^{-1})	-18	+6	-8
	$\Delta G^{\ddagger}$ (kcal.mol^{-1})	28	42	36
	ν (cm^{-1})	1824	1874	1855
with $PbOH^{+}$	ϵ_R^{ZPE} (a.u.)	-493.802	-493.808	-493.808
	ϵ_P^{ZPE} (a.u.)	-493.801	-493.797	-493.787
	ΔG (kcal.mol^{-1})	+1	+7	+14
	$\Delta G^{\ddagger}$ (kcal.mol^{-1})	35	41	45
	ν (cm^{-1})	1858	1866	1875

Figure 1. Proton transfers in uracil without lead (first row), uracil complexed with Pb^{2+} (second row), uracil complexed with $[Pb(H_2O)]^{2+}$ (third row), and uracil complexed with $[Pb(OH)]^{+}$ (fourth row). $N_3 \rightarrow O_8$ (first column), $N_1 \rightarrow O_7$ (second column), and $N_3 \rightarrow O_7$ (third row) proton transfers. The notations U_1, U_2, and U_4 are taken from ref 27 to designate the uracil tautomers obtained (independent of their coordination to lead) after the proton transfer has been achieved (proton transfer indicated by an arrow). Schemes at the top are drawn with a Pb^{2+} substituent, to be replaced by $[Pb(H_2O)]^{2+}$ and $[Pb(OH)]^{+}$, depending on the case under investigation.

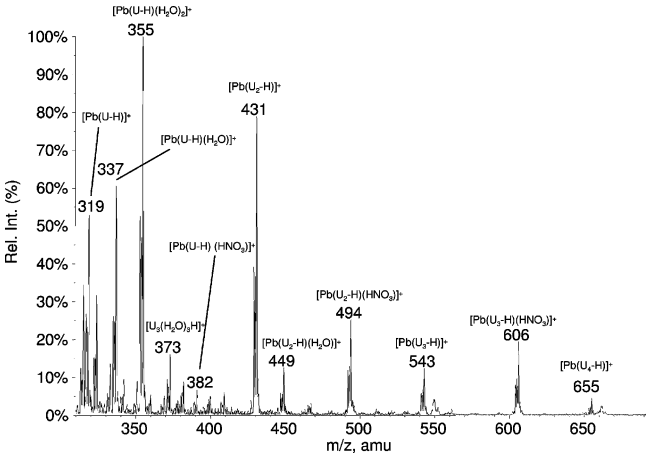

Figure 2. Positive ion electrospray source spectrum of uracil (10^{-3} mol L^{-1}) with $Pb(NO_3)_2$ (10^{-3} mol L^{-1}) in water.

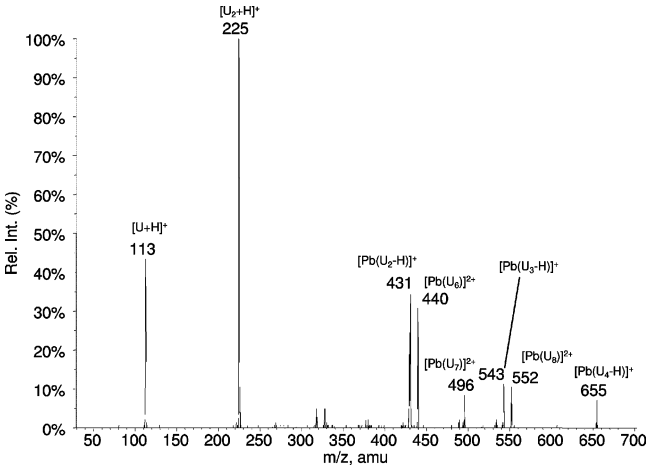

Figure 3. ESI MS/MS spectrum of $[Pb(U_8)]^{2+}$ ($m/z = 552$).

494, respectively. As an alternative demonstration of their existence in the beam, we have therefore recorded the MS/MS spectrum (at $m/z = 552$) corresponding to the heavy $[Pb(U_8)]^{2+}$ ion (see Figure 3). In addition, this spectrum gives the fragmentation patterns of the doubly charged species. Two dissociation channels are obtained: (i) The first is for doubly charged $[Pb(U_m)]^{2+}$ ($m = 7-6$) species, where the $[Pb(U_8)]^{2+}$ parent ion has lost up to two neutral uracil molecules (or uncharged fragments of uracil). See peaks related to $[Pb(U_7)]^{2+}$ and $[Pb(U_6)]^{2+}$ at $m/z = 496$ and 440, respectively. This nicely illustrates that doubly charged complexes can be produced upon

dissociation and fragmentation and remain energetically stable under our experimental conditions. As a remark, no $[Pb(U_m)]^{2+}$ ($m \leq 5$) species are detected, which suggests that such lighter species are not stable under the kinetic and thermodynamic conditions applied in the MS/MS experiment, displaying further chemical rearrangements and dissociations. (ii) The second dissociation channel corresponds to singly charged $[Pb(U_m)-H]^+$ and $[U_qH]^+$ ions, obtained through a dissociative proton transfer in $[Pb(U_m)]^{2+}$ (either in the parent molecule $[Pb(U_8)]^{2+}$ or in $[Pb(U_m)]^{2+}$ ($m < 8$) successive fragments). One can hence recognize peaks associated with the stable species $[UH]^+$, $[U_2H]^+$, $[Pb(U_2)-H]^+$, $[Pb(U_3)-H]^+$, and $[Pb(U_4)-H]^+$ at m/z = 113, 225, 431, 543, and 655, respectively. All these peaks were already recorded in the ESIMS source spectrum.

Our MS/MS experiments thus confirm that the production of singly charged ions $[Pb(U_m)-H]^+$ (or $[Pb(U_m)-H(H_2O)_p]^+$ or $[Pb(U_m)-H(HNO_3)_p]^+$) where uracil is deprotonated should stem from the formation of doubly charged species upon a dissociative proton-transfer mechanism. Here, we want to investigate such mechanisms and their related energetics and specifically quantify the role of lead binding. To that end, we follow two directions. On one hand, we will study proton transfers within the solvated species, as occurring in the water droplet initially formed in ESIMS. Typical species present in the water droplet are H_2O and OH^-; thus, we will be interested in the following reaction schemes: $[PbU]^{2+} + H_2O \rightarrow [Pb(U)-H]^+ + H_3O^+$ (scheme 1) and $[PbU]^{2+} + OH^- \rightarrow [Pb(U)-H]^+ + H_2O$ (scheme 2), where we have supposed that the intermolecular proton transfers in $[Pb(U_m)(H_2O)]^{2+}$ and $[Pb(U_m)(OH)]^{2+}$ involve only one uracil molecule, the others being weakly bonded spectators. On the other hand, we will study proton transfers within the gas-phase species, as occurring when all water molecules have evaporated. A scheme that would simultaneously account for the presence of $[Pb(U_p)-H]^+$ and $[U_qH]^+$ fragments in the experiment is a proton transfer between two weakly bonded uracil molecules in $[Pb(U_m)]^{2+}$ ions. Again, if we make the assumption that the proton transfer does in fact not need more than two uracil molecules to take place (the others being only spectators), the chemical reaction $[Pb(U_2)]^{2+} \rightarrow [Pb(U)-H]^+ + UH^+$ (scheme 3) may account for the proton transfer in any $[Pb(U_m)]^{2+}$ complex.

As already emphasized, metal chelation can also induce intramolecular proton transfers in the ligand, leading in our case to the formation of tautomeric forms of uracil. This will also be investigated in the present work. We are interested in uracil 1,3-proton transfers in doubly charged $[Pb(U)]^{2+}$ and singly charged $[PbOH(U)]^+$ gas-phase complexes, which are typical complexes present in our MS experiments. Comparison between doubly charged and singly charged complexes is aimed to demonstrate the role of the global charge in the proton transfer. We will also give some hints as to the role of a "microsolvation" of lead(II) by water in the uracil 1,3-proton transfers by studying $[Pb(H_2O)(U)]^{2+}$, where H_2O is attached to lead. Finally, we will emphasize 1,3-proton transfers mediated by a water molecule located at the proton site. In all of the studies, a series of working hypotheses (that will be presented in due course) will be made. We thus do not pretend to give an exhaustive view of all possibilities related to proton-transfer schemes, but rather, we present selected schemes that illustrate our aim (i.e., the assessment of the role of lead in proton transfers).

The paper is organized as follows. Computational details on the quantum calculations are presented in section 2. Calculations on uracil 1,3-intramolecular proton-transfer events are presented in sections 3.1−3.4 with the $[Pb(U)]^{2+}$, $[Pb(H_2O)(U)]^{2+}$, $[Pb(U)(H_2O)]^{2+}$, and $[PbOH(U)]^+$ systems, respectively. Calculations on intermolecular proton transfers are reported in sections 3.3−3.5, according to the reactions $[Pb(U)]^{2+} + H_2O \rightarrow [Pb(U-H)]^+ + H_3O^+$, $[Pb(U)]^{2+} + OH^- \rightarrow [Pb(U-H)]^+ + H_2O$, and $[PbU_2]^{2+} \rightarrow [Pb(U-H)]^+ + UH^+$. We have calculated potential energy surfaces (PES) with predefined reaction coordinates in sections 3.3 and 3.5. In section 3.5, as enol tautomers are highly reactive nucleophiles, we have investigated uracil dimers composed of oxo/hydroxo molecules. All studies have been performed with and without lead(II) to fully quantify the role of the metal cation in the proton-transfer processes. Conclusions are presented in section 4.

2. Computational Details and Notations

Calculations have been performed with the Gaussian-98[21] set of programs. As in ref 12, the inner electronic structure of lead ($[Xe]4f^{14}5d^{10}$) has been described with the "Stuttgart" quasi-relativistic pseudopotential developed by Küchle et al.[22] The outer electrons of lead have been explicitly accounted for with the (4s,4p,1d)/[2s,2p,1d] basis set with a (3,1) contraction scheme for s and p functions. All electrons of C, N, O, and H atoms have been described by the standard 6-31G(d,p) Pople basis set. We have used the spin-unpolarized B3LYP density functional. We have chosen this computational setup on the basis of previous works.[9,23,24] In particular, we have demonstrated that the effect of an extended basis set for Pb (developed to be used with the Stuttgart effective core potential) on the height of activation barriers is small (few kJ/mol). Because the crucial point of the present investigation is actually the height of activation barriers, we decided to stick to the B3LYP/6-31G(d,p) level.

For a given reaction, geometry optimizations have been performed on the so-called reactants, products, and transition states and supplemented with harmonic vibrational frequencies. We provide (a) potential energies with ZPE corrections (ϵ^{ZPE}) for stationary points and (b) Gibbs free energies with thermal corrections for the transformations reactants → products (ΔG) and reactants → transition state ($\Delta G^{\ddagger}$). The approximations for all corrections are those implemented in Gaussian.[25] Data (a) have been used to compare the stability of isomers. Data (b) have been used to estimate the thermodynamics of the reactions as well as their kinetic rate constants (k) on the basis of the activated complex theory.[26] Rate constants are calculated by $k = k_B T/h(RT)^{-\Delta n} e^{-\Delta G^{\ddagger}/(RT)}$, where k_B is the Boltzmann factor, h is Planck's constant, R is the ideal gas constant, T is the temperature, and Δn is the variation in the number of molecules in the reaction. Half-reaction times ($\tau_{1/2}$) have also been calculated. In the case of bimolecular processes, the initial concentrations of the two reactants have been taken as 10^{-3} mol L^{-1}. This is an arbitrary value chosen to give an order of magnitude for $\tau_{1/2}$, and as we will see later, slightly different values would not change the final conclusions.

We have also calculated bidimensional potential energy surfaces, without ZPE corrections (ϵ). These surfaces help to visualize the proton-transfer paths and ease the comparisons between the different envisioned reactions. Two reaction coordinates were systematically used: the bond length connecting the proton to be transferred to its donor atom (N) and the bond length to its acceptor atom (O or N, depending on the acceptor molecule). These bond lengths have been monitored between 1.0 and 2.5 Å (with an increment of 0.1 Å); all other degrees of freedom were optimized.

The atom numbering used for uracil throughout the text is given in Figure 4. We will often refer to the diamide uracil

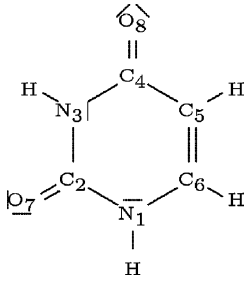

Figure 4. Atom numbering for uracil.

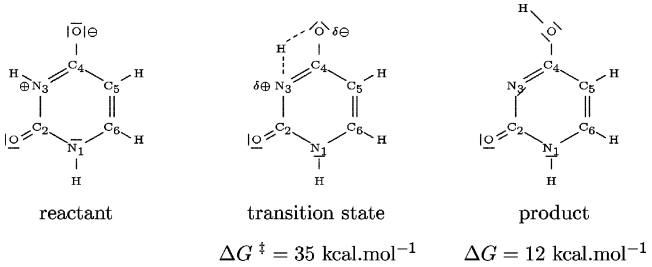

Figure 5. $N_3 \rightarrow O_8$ proton transfer in oxo uracil.

tautomer (lactam) as the "oxo" (ketonic) form and to a tautomer containing one imino-alcohol group (lactim) as a "hydroxo" (enolic) form. We will also be speaking of 1,3-proton transfer in uracil, in terms of $N_1 \rightarrow O_7$, $N_3 \rightarrow O_7$, and $N_3 \rightarrow O_8$ transfers. These notations mean that the proton attached to the N_1 (or N_3) atom of uracil will be transferred to the adjacent carbonyl O_7 (or O_8) oxygen. Once the proton transfer has been achieved, the uracil nucleobase is said to adopt one of its enol tautomeric forms (denoted as U1, U2, or U3 following the notations of ref 27).

The following discussions will always be organized into two parts: one related to the reactivity without lead and one related to the reactivity with lead. Comparison of the results will assess the role of lead.

3. Results and Interpretations

3.1. Proton Transfers within Gaseous $[Pb(U)]^{2+}$ Ions. *Reactivity without Lead.* Up to 13 uracil tautomers, some of them close in energy, have been characterized in the literature.[27−32] Here, we are only interested in tautomers that can be involved in $N_1 \rightarrow O_7$, $N_3 \rightarrow O_7$, or $N_3 \rightarrow O_8$ 1,3-proton transfers and in seeing how the reactivity is modified by the presence of lead. All our results concerning the formation of tautomers U2 ($N_3 \rightarrow O_8$), U1 ($N_1 \rightarrow O_7$), and U4 ($N_3 \rightarrow O_7$) (U1, U2, and U4 are chosen according to the notations of ref 27) are given in Figure 1 (first row). As an illustration, a scheme is also given in Figure 5 for one of the mechanisms of interest (i.e., the $N_3 \rightarrow O_8$ proton transfer giving rise to tautomer U2). To our knowledge, few studies mention the transition state connecting a given uracil tautomer to another one.[33,34] Intramolecular 1,3-proton-transfer mechanisms in uracil are known to involve σ orbitals in the plane of the ring, so accordingly, we have investigated in-plane proton transfers. We found, in qualitative agreement with refs 33 and 34, that reaching the transition state requires as much as $\Delta G^{\ddagger} = 35$, 36, and 41 kcal mol^{-1} for the $N_3 \rightarrow O_8$, $N_1 \rightarrow O_7$, and $N_3 \rightarrow O_7$ proton transfers, respectively. The corresponding estimations for the rate constants (k) and half-reaction times ($\tau_{1/2}$) are $k = 1 \times 10^{-13}$, 2×10^{-14}, and 5×10^{-18} s^{-1} and $\tau_{1/2} = 5 \times 10^{12}$, 3×10^{13}, and 1×10^{17} s, respectively, which can be considered "geological" time scales. Imaginary frequencies of the transition states are 1854, 1848, and 1858 cm^{-1}. These reactions are endergonic by 12, 11, and 20 kcal mol^{-1}, respectively. Hydroxo tautomers are thus energetically disfavored with respect to the oxo tautomers, with huge kinetic energy barriers to produce them. Moreover, as the products are higher in energy than the reactants, we are in a case where the Hammond postulate is satisfied (i.e., transition states resemble product states). Therefore, the kinetic ordering of the three reactions investigated here follows the stability ordering of the products: the two uracil tautomers of lower energy, U_1 and U_2, are at the same time those requiring the least amount of energy to be produced (36 and 35 kcal mol^{-1}, respectively). (Note the following restriction. The energies of U_1 and U_2 are in the range of 1 kcal mol^{-1}. Their relative energy order cannot therefore be clearly stated at the present level of calculation. In ref 27, the ordering is reversed by changing the calculation method from B3LYP to CCSD.) In contrast, the monohydroxy tautomer U_4, which lies at an even higher energy than the dihydroxy tautomer U_3, requires as much as 41 kcal mol^{-1} to be produced.

One last comment on the in-plane 1,3-proton transfers should be given. This planar symmetry stems from the fact that the nitrogen proton donor of the amide group is sp^2 hybridized; as a consequence, any out-of-plane distortion of the corresponding N−H bond to achieve 1,3-proton transfer is expected to be more costly than the in-plane mechanism. Our results can be further understood by comparison with proton transfers in simpler molecular systems. The largest activation energy obtained here (41 kcal mol^{-1} for the $N_3 \rightarrow O_7$ proton transfer) is equal to that required to tautomerize the formamide molecule ($HCONH_2$) (at the same level of calculation). Accordingly, it can be concluded that ring aromaticity plays a very small role in the uracil proton-transfer mechanism, which arises outside of the ring. The transfer of a hydroxyl proton in formic acid (HCOOH) is slightly less expensive (29 kcal mol^{-1}) than the transfer energy value we obtained here for uracil. In contrast, the transfer of a methyl proton in formaldehyde ($HCOCH_3$) costs as much as 65 kcal mol^{-1}. This value is particularly large due to the participation of the π orbitals in the reaction. (Because the methyl carbon is sp^3-hybridized, the C−H bond is found to be slightly out-of-plane in the transition state.)

Reactivity with Lead. Unlike benzene,[35] the electrostatic potential of uracil is positive over the entire ring region, and it is negative only on the external carbonyl oxygens. Accordingly, lead is found to be monocoordinated with one of the carbonyl oxygens (O_7 or O_8) in the dication $[Pb(U)]^{2+}$, resulting in $\epsilon^{ZPE} = -417.533$ or -417.551 au when binding to O_7 and to O_8, respectively (see Figure 1). We decided to investigate 1,3-proton transfers involving a free oxygen (O_7 if O_8 is coordinated to lead and O_8 if O_7 is coordinated to lead) and a proton coming from an adjacent NH amide group (N_1 or N_3). Our argument to justify that restriction is that H^+ and Pb^{2+} both coordinated to the same carbonyl oxygen would give rise to high electrostatic repulsions, even if the charge of the oxygen is made more negative by such a cationic environment. The following situations are considered: $N_3 \rightarrow O_8$ proton transfer if lead is coordinated with O_7 (reaction 1) and $N_3 \rightarrow O_7$ and $N_1 \rightarrow O_7$ proton transfers if lead is coordinated with O_8 (reactions 2 and 3, respectively). Reaction 1 is schematized in Figure 6 to illustrate the discussion, and all results are reported in Figure 1 (second row).

We found that proton transfers still occur in the uracil plane in the presence of lead. $N_3 \rightarrow O_8$ proton transfer (reaction 1) is now made easier by the presence of lead. Of course, the activation energy barrier remains high (29 kcal mol^{-1}), but it has been lowered by 6 kcal mol^{-1} from the situation where lead

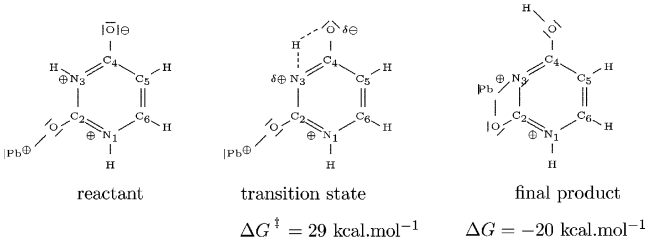

Figure 6. $N_3 \rightarrow O_8$ proton transfer in oxo uracil complexed with Pb^{2+} at position O_7.

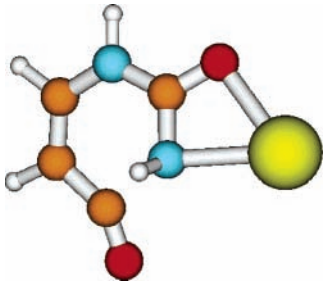

Figure 7. Transition state for opening the uracil cycle ($\Delta G^{\ddagger} = 19$ kcal mol^{-1}, $\nu = 258$ cm^{-1}). Nitrogen atoms are in blue, carbons in orange, oxygens in red, hydrogens in gray, and lead in yellow.

was not present (see Figure 1, first row). More remarkably, the reaction becomes exergonic by 20 kcal mol^{-1} when lead is present instead of being endergonic ($\Delta G = 12$ kcal mol^{-1}) without lead. $N_3 \rightarrow O_7$ proton transfer (reaction 2) exhibits the same trends, though slightly attenuated: the activation energy barrier is lowered by 5 kcal mol^{-1}, and the reaction becomes exergonic by 8 kcal mol^{-1}. In contrast, the energy balance of $N_1 \rightarrow O_7$ proton transfer is endowed (reaction 3): the activation energy barrier is increased by 6 kcal mol^{-1}, and the endergonicity is only reduced to 5 kcal mol^{-1}. Saddle points correspond to the proton departure without any involvement of Pb^{2+}, with imaginary frequencies of 1836, 1872, and 1870 cm^{-1} for reactions 1, 2, and 3, respectively.

Exergonicity and endergonicity can be understood from mechanistic features. Once the transition state has been reached and the proton transferred, the system evolves barrierlessly toward a structure where lead becomes bicoordinated to N_3 and O_8 (reaction 1) or to N_3 and O_7 (reaction 2; see Figure 6 for an illustration). This is not the case with reaction 3 where bicoordination of lead to O_8 and N_3 is not allowed, because of the N_3 site still being protonated. Therefore, the reaction is thermodynamically favored when lead has the opportunity to bicoordinate to neighboring O and N atoms, after the nitrogen site has been freed (reactions 1 and 2). Otherwise (reaction 3), it is thermodynamically as disfavored as when lead was not present. Kinetics remains nonetheless extremely slow in all cases, as estimated by rate constants and half-reaction times: $k = 3 \times 10^{-9}$, 9×10^{-19}, and 2×10^{-14} s^{-1} and $\tau_{1/2} = 2 \times 10^{8}$, 7×10^{17}, and 3×10^{13} s for reactions 1, 2, and 3, respectively.

Let us end the section by recording an alternative mechanism to the proton transfer in the presence of lead. See Figure 7 for an illustration of the transition state of this mechanism. In this state, we found that once lead has been attached to the O_7 carbonyl oxygen, it can coordinate at the same time to the neighboring N_3 (which still bears its proton but not lying in the plane of uracil anymore). Moreover, N_3 recovers its electronic valency by breaking the N_3C_4 bond. In that case, the $N_3 \rightarrow O_8$ proton transfer does not occur, and the aromatic cycle is opened instead. As can be seen from a reverse IRC analysis, this transition state is connected to the same reactant structure as

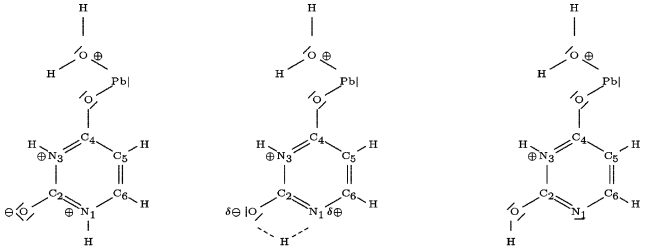

Figure 8. $N_1 \rightarrow O_7$ proton transfer in oxo uracil complexed with $[Pb(H_2O)]^{2+}$ at position O_8.

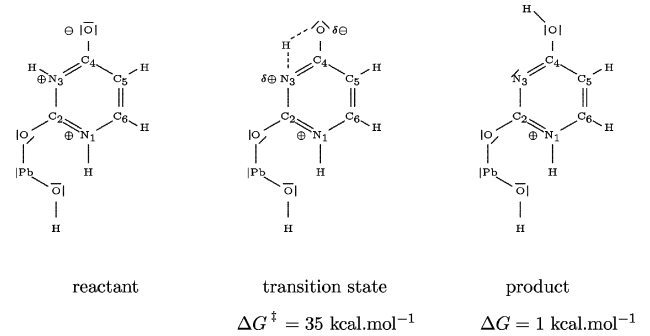

Figure 9. $N_3 \rightarrow O_8$ proton transfer in oxo uracil complexed with $[Pb(OH)]^{+}$ at position O_7.

for $N_3 \rightarrow O_8$ proton transfer. As a result, the barrier heights of both reactions can be compared. We have found $\Delta G^{\ddagger}$ values of 19 (associated with $k = 0.1$ s^{-1} and $\tau_{1/2} = 6$ s) and 35 kcal mol^{-1} for the opening of the cycle and the $N_3 \rightarrow O_8$ proton transfer, respectively, showing that the ring opening is energetically more favorable. Very nicely, this result can be put in perspective with the "activation" of the N_3C_4 bond of uracil by lead(II), which was noticed in our previous study.[12]

3.2. Role of Lead Microsolvation. Our purpose is to find out how these proton transfers are modified when one water molecule is added to Pb^{2+}, either in its nonhydrolyzed $[Pb(H_2O)]^{2+}$ form or in its hydrolyzed $[Pb(OH)]^{+}$ form. We will investigate the same proton transfers as in section 3.1, replacing Pb^{2+} by $[Pb(H_2O)]^{2+}$ or $[Pb(OH)]^{+}$. With such simple models of "lead microsolvation", we expect to get upper bounds to the energies involved in bulk solvent (where more degrees of freedom are available to relax chemical rearrangements). Our results are summarized in Figure 1 (third and fourth rows), and illustrations are schematized in Figures 8 and 9.

We found that microsolvating Pb^{2+} with one water molecule does not change the general trends previously obtained with Pb^{2+} alone. The exergonic property of the $N_3 \rightarrow O_8$ and $N_3 \rightarrow O_7$ proton transfers is still present ($\Delta G = -18$ kcal mol^{-1} and $\Delta G = -8$ kcal mol^{-1}, respectively), and the endergonicity of the $N_1 \rightarrow O_7$ proton transfer reaction is slightly increased from that obtained with Pb^{2+} ($\Delta G = 6$ kcal mol^{-1}). In contrast, we found more drastic changes with $[Pb(OH)]^{+}$ with respect to Pb^{2+}. If $N_1 \rightarrow O_7$ proton transfer is nearly as disfavored ($\Delta G = 7$ kcal mol^{-1}) as it was with Pb^{2+} ($\Delta G = 5$ kcal mol^{-1}), the exergonicity of $N_3 \rightarrow O_8$ and $N_3 \rightarrow O_7$ proton transfers is lost ($\Delta G = 1$ kcal mol^{-1} and $\Delta G = 14$ kcal mol^{-1}, respectively). Note that ΔG of the $N_3 \rightarrow O_8$ reaction is at the frontier between exergonicity and endergonicity, at the present level of calculation. In any case, these results assess the role of the global charge of lead in the 1,3-proton-transfer events.

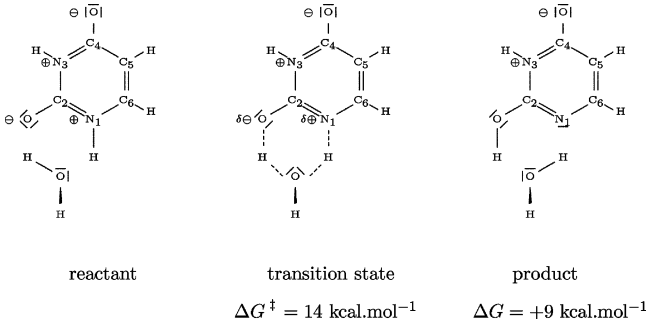

Figure 10. $N_1 \rightarrow O_7$ proton transfer in oxo uracil mediated by a water molecule bridging the N_1-H and O_7 sites.

3.3. Role of Microsolvation of the Uracil Proton-Transfer Site. Contrary to the previous section, we now deal with the $[Pb(U)(H_2O)]^{2+}$ ion where the water molecule is located at the proton-transfer site. Two data types will be dealt with: (a) stationary points, if there are any on the reaction path, and (b) bidimensional potential energy surfaces, as they supply reactivity information even in the absence of stationary points. See section 2 for computational details.

Reactivity without Lead. Although numerous theoretical studies[31,33,36−39] have characterized the most stable structures of uracil complexed with one water molecule, very few have dealt with uracil 1,3-proton-transfer reactions catalyzed by this water molecule.[33] This is our point here. As shown in the literature, water bridges adjacent N−H and C═O sites of uracil through two intermolecular hydrogen bonds in oxo(U)−water dimers. Three such bridges are encountered, $N_1-H/C_2{=}O_7$ (complex denoted U-W-1), $N_3-H/C_4{=}O_8$ (complex denoted U-W-2), and $N_3-H/C_2{=}O_7$ (complex denoted U-W-3). In these structures, water is in a position to mediate proton transfers, from N_1 to O_7, N_3 to O_8, or N_3 to O_7, respectively. As an illustration, the proton transfer occurring in the U-W-1 complex has been schematized in Figure 10. We obtained proton-transfer free energies of $\Delta G = 9$, 8, and 14 kcal mol^{-1} and activation free energies of $\Delta G^{\ddagger} = 14$, 14, and 13 kcal mol^{-1} for $N_1 \rightarrow O_7$ (illustrated in Figure 10), $N_3 \rightarrow O_8$, and $N_3 \rightarrow O_7$, respectively. These values yield rate constants and reaction half-times of $k = 235$, 168, and 1276 mol^{-1} L^{-1} s^{-1} and $\tau_{1/2} = 4$, 6, and 1 s, respectively. Uracil tautomerization mediated by one water molecule is thus very fast at room temperature, and all the more within the ESIMS and MS/MS experimental conditions. Imaginary frequencies of the transition states are 1440, 1345, and 1394 cm^{-1}, respectively. They are attributed to a concerted process where a nitrogen uracil proton is given to water; in contrast, the water molecule gives another proton back to the neighboring carbonyl oxygen of uracil (see illustration in Figure 10). These reactions are nonetheless endergonic.

We have gone one step further and have calculated the bidimensional potential energy surface (PES) of the water-mediated $N_1 \rightarrow O_7$ proton transfer. The PES is plotted in Figure 11(left part). (We recall that the corresponding mechanism is schematized in Figure 10.) In our calculations, the uracil N_1H and the water OH bond lengths (bond lengths that are indeed deeply modified during the tautomerization process) are evolved between 1.0 and 2.5 Å (in 0.1 Å increments), and all other degrees of freedom are optimized. The lowest well corresponds to the oxo uracil doubly hydrogen bonded with water ($\epsilon_{OH=1.0}^{N_1H=1.0} = -491.268$ au). A secondary and flat well corresponds to the hydroxo uracil doubly hydrogen bonded with water ($\epsilon_{OH=1.9}^{N_1H=1.7} = -491.255$ au) and lies 8 kcal mol^{-1} higher in energy than the former one. Two types of paths can be followed to connect these two wells, with either concerted or stepwise mechanisms. Along the concerted path (where N_1H and OH bonds are lengthened simultaneously), the highest structure that can be reached (with $N_1H = 1.3$ Å, OH = 1.3 Å) lies 16 kcal mol^{-1} above the lowest minimum ($N_1H = 1.0$ Å, OH = 1.0 Å). Comparatively, along the two possible stepwise paths (uracil deprotonation by water and then release of that proton to uracil oxygen, or protonation of uracil oxygen by water and then uracil deprotonation to regenerate water), the highest structures to be reached (corresponding to ($N_1H = 1.7$ Å, OH = 1.0 Å) and ($N_1H = 1.0$ Å, OH = 1.7 Å), respectively) are much higher in energy (25.0 and 38.5 kcal mol^{-1}, respectively) than the lowest minimum ($N_1H = 1.0$ Å, OH = 1.0 Å).

Reactivity with Lead. We now investigate the water-mediated $N_1 \rightarrow O_7$ proton transfer with lead bonded to O_8. This situation can be denoted as "para" and has been schematized in Figure 12. Note that in all other configurations, water is captured by lead, and hence, it can no longer be used as a proton carrier. The proton transfer is now associated with $\Delta G = 1$ kcal mol^{-1} and $\Delta G^{\ddagger} = 2$ kcal mol^{-1}, yielding $k = 3 \times 10^{11}$ mol^{-1} L^{-1} s^{-1} and $\tau_{1/2} = 3 \times 10^{-9}$ s. The proton-transfer reaction is therefore faster than without lead. Moreover, the endergonicity of the reaction is almost lost, at the present level of calculation. Interestingly, as seen on the potential energy surface (Figure 11, right), the reactant well now corresponds to a structure where uracil is only singly hydrogen bonded to water ($N_1H = 1.1$ Å, OH = 1.0 Å). Consequently, the lowest energy path connecting the reactant and product wells corresponds to a stepwise mechanism. As a first step, the uracil N_1H site is deprotonated by water to form H_3O^+. As a second step, H_3O^+ gives another proton to the neighboring carbonyl oxygen O_7. The proton-transfer reaction is found to be slightly endothermic ($\Delta\epsilon_{OH=1.0\rightarrow1.4}^{N_3H=1.1\rightarrow2.5} = 2$ kcal mol^{-1}). Let us emphasize that escape of H_3O^+ from the deprotonated leaded uracil (after the first step) gives rise to the $[Pb(U)-H]^+$ ion, which is indeed observed in our mass spectrometry measurements.

We now consider the water-mediated $N_3 \rightarrow O_8$ proton transfer, when lead is connected to O_7. In this situation, water and lead are located closer to each other than in the previous case. This situation can now be denoted as "ortho". As mentioned previously, optimization of all degrees of freedom but the reaction coordinates (N_3H and OH) gives rise to the $[(Pb(H_2O))(U)]^{2+}$ ion (already studied), where lead and water have formed a $Pb(H_2O)^{2+}$ complex H-bonded to uracil. To avoid this unwanted event, we have fixed the distance between the water oxygen and lead to 5.7 Å. (We have made two separate geometry optimizations: $[Pb-uracil]^{2+}$, in which Pb^{2+} is monocoordinated to O_7, and uracil$-H_2O$, where the water molecule is H-bonded to the N_3 and O_8 sites. We have subsequently combined both geometries and found that the distance between Pb^{2+} and the oxygen of the water molecule is approximately 5.7 Å. Accordingly, we have fixed that distance to 5.7 Å to generate the structures in the potential energy surface at the bottom of Figure 11. One should be reminded that without fixing that distance, Pb^{2+} is strongly attracted by the water molecule, so as to form one $Pb(H_2O)^{2+}$ complex, which would prevent the proton transfer from being observed.) The resulting "biased" potential energy surface has been plotted at the bottom of Figure 11. Remarkably, the reactant structure ($N_3H = 1.0$ Å, OH = 1.0 Å) is no longer associated to a minimum on the potential energy surface, and it evolves barrierlessly and exothermically toward the hydroxo tautomer of leaded uracil weakly bonded to water ($N_3H = 2.5$ Å, OH = 1.5 Å). The energy difference between the reactant and product is $\Delta\epsilon_{OH=1.0\rightarrow1.5}^{N_3H=1.0\rightarrow2.5} = -15$ kcal

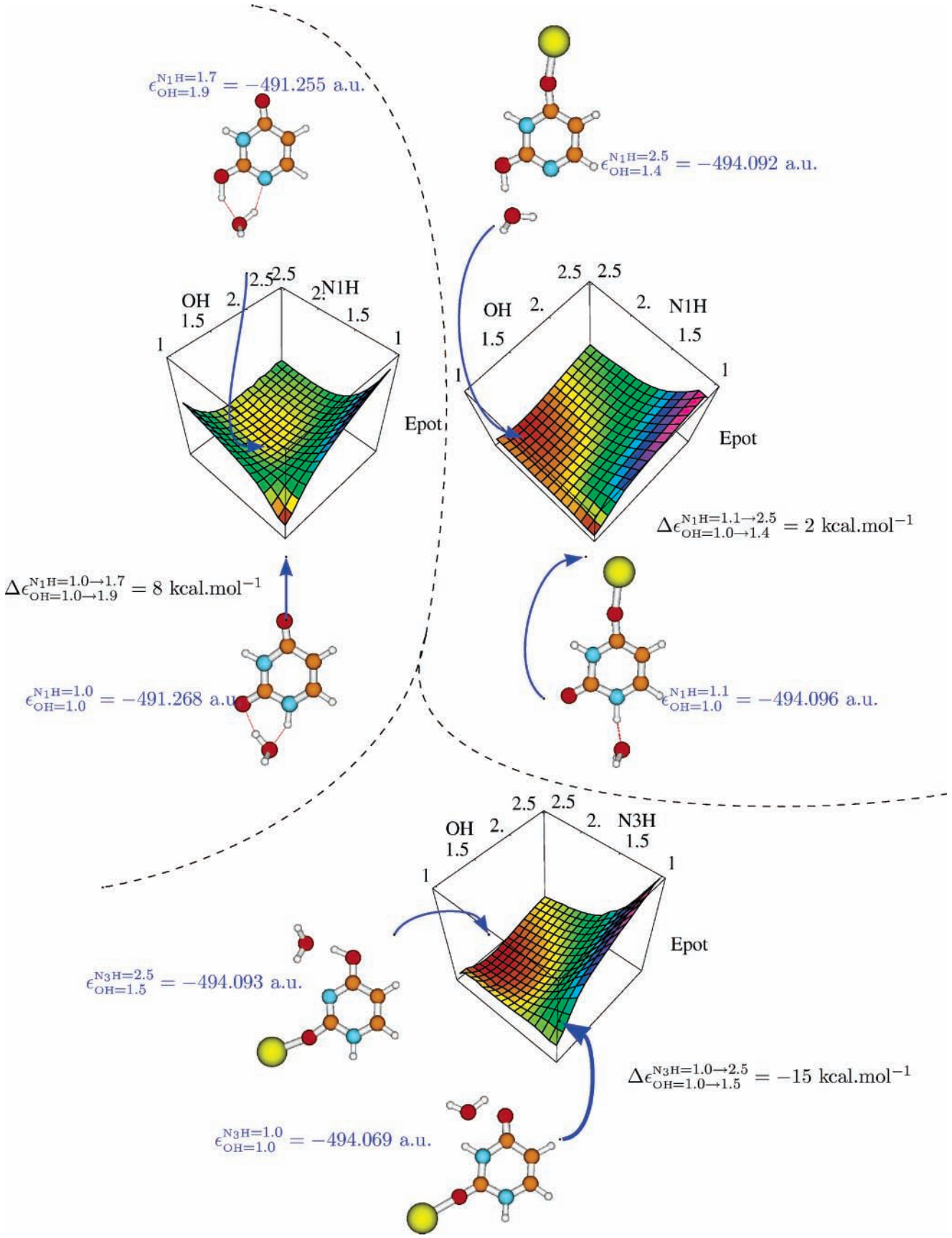

Figure 11. Bidimensional potential energy surfaces for water-mediated uracil 1,3-proton transfers. Top: $N_1 \rightarrow O_7$ without lead (left), with lead (right) bonded to O_8. Bottom: $N_3 \rightarrow O_8$ with lead bonded to O_7. The potential energy is increasing from red to blue. Two geometry parameters are chosen to monitor the proton transfer from a nitrogen to an oxygen: the lengths of uracil NH and water OH bonds that are deeply modified by the proton transfer (see text for explanations). Typical notations: $\epsilon^{N_1H=1.0}_{OH=1.0}$ designates the electronic energy of the structure where N_1H and OH bond lengths are both 1.0 Å and $\Delta\epsilon^{N_1H=1.0\rightarrow1.7}_{OH=1.0\rightarrow1.9}$ is the energy of the transformation from the structure having $N_1H = 1.0$ Å and OH = 1.0 Å to the structure having $N_1H = 1.7$ Å and OH = 1.9 Å.

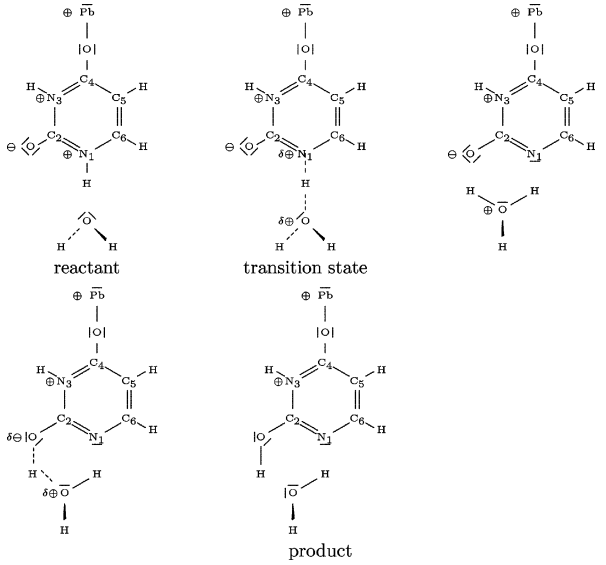

Figure 12. $N_1 \rightarrow O_7$ proton transfer in oxo uracil complexed with Pb^{2+} at position O_8 mediated by a water molecule bridging N_1-H and O_7 sites.

mol^{-1}. Again, the lowest energy path for this proton transfer agrees with a stepwise mechanism: N_3H is deprotonated by water to form H_3O^+, and then H_3O^+ gives another proton back to O_8. Again, after the first step has been completed, an escape of H_3O^+ gives rise to the experimentally observed $[Pb(U)-H]^+$ ion.

As a final remark, $N_3 \rightarrow O_8$ proton transfer would have been even more exergonic if lead had been allowed to bicoordinate to O_7 and N_3 at the end of the reaction. From a thermodynamic point of view, this case is very similar to those of section 3.1, where the proton transfer was studied without water mediation.

3.4. OH^- as a Proton Acceptor in Uracil 1,3-Proton Transfers. During electrospray experiments,[12] OH^- ions are likely to be formed. In regard to our theoretical calculations, we found that uracil can be easily deprotonated by OH^- (strong base), and the process is barrierless and exergonic. As an example, let us consider the deprotonation of N_1H when OH^- is bonded to it. We have calculated the following Gibbs free energies for isolated uracil, isolated OH^-, and deprotonated N_1 uracil interacting with one water molecule: −414.761, −75.735, and −490.640 au, respectively. By starting with the reactants at infinite separation, the deprotonation reaction releases as much as $\Delta G = -91$ kcal mol^{-1}. With lead, the reaction is even more exergonic. For instance, let us consider the deprotonation of N_1H, lead being complexed to O_8. The Gibbs free energies involved are −417.588, −75.735, and −493.729 au for isolated $[Pb(U)]^{2+}$, isolated OH^-, and $[Pb(U)-H]^+$, respectively, interacting with water. The exergonicity of the proton transfer in leaded uracil is now $\Delta G = -255$ kcal mol^{-1}.

3.5. Uracil−Uracil Intermolecular Proton Transfers. In this section, we present mechanisms involving uracil dimers to study $[Pb(U_2)]^{2+} \rightarrow [Pb(U)-H]^+ + [UH]^+$ proton-transfer reactions. We consider reactants in which lead is complexed to one uracil only. On the basis of refs 40−42, we excluded geometries of stacked uracil dimers and we only considered two uracils located within the same plane. In fact, one can infer that a proton can hardly be transferred between two stacked uracils without the help of a third molecule, and here, we focus on bimolecular processes at most. As a final working hypothesis, we considered that the reactivity of the uracil dimer is increased when one of the two monomers is composed of a uracil hydroxo

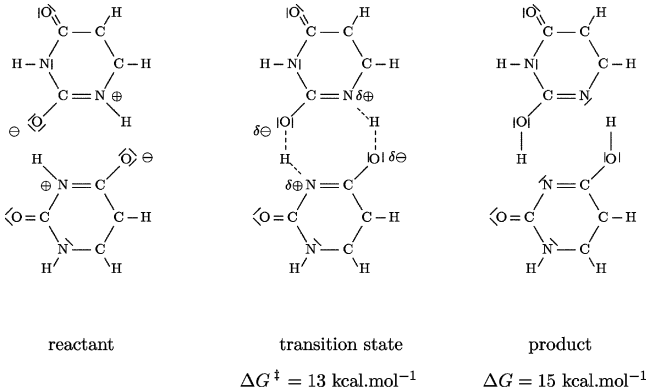

Figure 13. oxo(U)−oxo(U) coplanar double enolization.

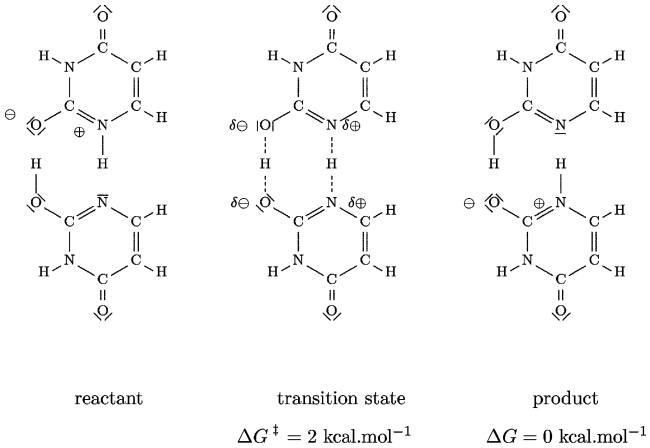

Figure 14. oxo(U)−hydroxo(U) coplanar double proton transfer.

tautomer. Two arguments support this assumption. First, as previously seen, hydroxo tautomers are easily and quickly formed at ambient temperature provided that a water molecule or a OH^- ion participates in the proton-transfer reaction. This favorable process is likely to occur during our MS experiments, where the reactive species are formed in aqueous solution. Second, hydroxo tautomers are better proton acceptors than oxo tautomers. As an illustration, we propose to compare the kinetics of a double proton-transfer reaction either involving two oxo uracils (Figure 13) or one oxo uracil bonded to one hydroxo tautomer (Figure 14). An activation energy of $\Delta G^{\ddagger} = 13$ kcal mol^{-1} is obtained in the former case, against only 2 kcal mol^{-1} in the latter case. Moreover, if the oxo−oxo proton transfer is endergonic, this is not the case anymore when one uracil adopts one of its hydroxo tautomeric forms (see ΔG values written in Figures 13 and 14). In the following, the $[Pb(U_2)]^{2+} \rightarrow [Pb(U)-H]^+ + [UH]^+$ proton-transfer reactions will be therefore investigated considering oxo−hydroxo uracil dimers, as the presence of one hydroxo uracil energetically favors intermolecular proton transfers.

Reactivity without Lead. We restrict our investigation to the $N_1 \rightarrow N_1$ proton transfer in singly hydrogen bonded oxo(U)−hydroxo(U) reactants, as illustrated in Figure 15. Moreover, the uracil dimer is assumed to be hydrogen bonded through one H-bond only, namely N1−H···N1. The bidimensional potential energy surface of oxo(U)−hydroxo(U) has been plotted in Figure 15 (top left). One should remember that the energy is monitored along two reaction coordinates, namely the two distances between the proton to be transferred and the N_1 atom of each uracil; all other degrees of freedom are optimized. These nitrogens are hereafter denoted as N_{1t} and N_{1b} for top and bottom rings, respectively. The main representative structures of the

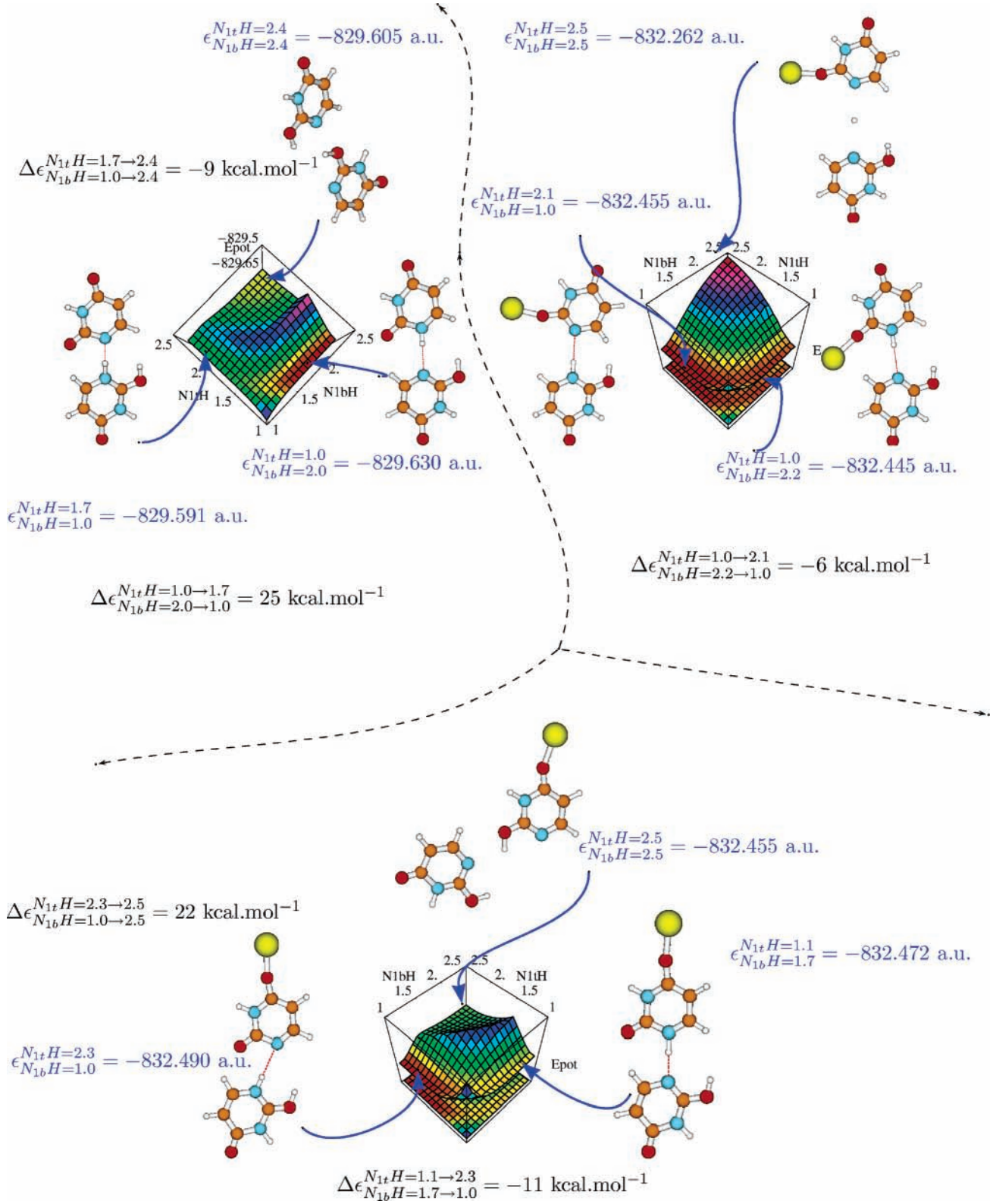

Figure 15. Bidimensional potential energy surfaces for $N_{1t}-H \rightarrow N_{1b}$ proton transfer in oxo(U)−hydroxo(U). Top: without lead (left), with lead (right) bonded to O_7 of oxo uracil. Bottom: with lead bonded to O_8 of oxo uracil. The potential energy is increasing from red to blue. See also the legend of Figure 11 and the text for explanations. Two geometry parameters are chosen to monitor the proton transfer from the the N_1 nitrogen (N_{1t}) of the cycle on top of the dimer to the N_1 nitrogen (N_{1b}) at the bottom of the dimer: $N_{1t}H$ and $N_{1b}H$ bond lengths. Typical notations: $\Delta\epsilon^{N_{1t}H=1.7}_{N_{1b}H=1.0}$ designates the electronic energy of the structure where $N_{1t}H$ and $N_{1b}H$ bond lengths are 1.0 and 1.7 Å, respectively, and $\Delta\epsilon^{N_{1t}H=1.0\rightarrow1.7}_{N_{1b}H=2.0\rightarrow1.0}$ is the energy of the transformation from the structure having $N_{1t}H = 1.0$ Å and $N_{1b}H = 2.0$ Å to the structure having $N_{1t}H = 1.7$ Å and $N_{1b}H = 1.0$ Å.

dimer are represented in the figure, to be discussed in the text. The absolute minimum has been attributed to oxo(U) singly hydrogen bonded to hydroxo(U) through $N_{1t}H_1\cdots N_{1b}$. This structure is characterized by the coordinates $N_{1t}H = 1.0$ Å and $N_{1b}H = 2.0$ Å, and it lies in a narrow basin spreading along the $N_{1b}-H_1$ coordinate. A flatter energy basin of higher energy is obtained for the two weakly interacting hydroxo(U) (each N_1H coordinate $\sim$ 2.4 Å). This secondary minimum lies

$\Delta\epsilon^{N_{1t}H=1.0\rightarrow2.4}_{N_{1b}H=2.0\rightarrow2.4} = +15.6$ kcal mol^{-1} higher in energy above the main minimum. The lowest energy path connecting these two minima corresponds to a stepwise mechanism. In a first step, $N_{1t}H$ is elongated and $N_{1b}H$ shortened. As an indication, the transformation from ($N_{1t}H = 1.0$ Å, $N_{1b}H = 2.0$ Å) to ($N_{1t}H = 1.7$ Å, $N_{1b}H = 1.0$ Å) (which does not lead to a minimum) requires as much as $\Delta\epsilon^{N_{1t}H=1.0\rightarrow1.7}_{N_{1b}H=2.0\rightarrow1.0} = 25$ kcal mol^{-1}. This energy value would give rise to $\tau_{1/2}$ greater than 10^8 s, corresponding to a slow process. In contrast, the second step from ($N_{1t}H = 1.7$ Å, $N_{1b}H = 1.0$ Å) to ($N_{1t}H = 2.4$ Å, $N_{1b}H = 2.4$ Å) releases $\Delta\epsilon^{N_{1t}H=1.7\rightarrow2.5}_{N_{1b}H=1.0\rightarrow2.5} = -9$ kcal mol^{-1}. Once the proton has been transferred from the oxo to the hydroxo uracil, the resulting dimer of oxo $[U-H]^-$ and hydroxo $[UH]^+$ is further stabilized by an approximate 90° rotation of the two rings in the same plane. In that way, the just protonated hydroxo uracil easily gives back its N_1H proton to the O_7 oxo uracil site, which leads to the final dimer composed of two hydroxo(U). This stabilization can be attributed to the position of the enol proton that is surrounded by three nucleophilic sites: N_{1t}, N_{1b}, and O_7.

Reactivity with Lead. We have investigated two complexation sites for lead (i.e., O_7 and O_8) (Figure 15, top right and bottom right, respectively). We will first comment on Figure 15, top right (lead connected to O_7). Unlike the situation without lead, $[Pb-oxo(U)]^{2+}$ hydrogen bonded to hydroxo(U) ($N_{1t}H = 1.0$ Å, $N_{1b}H = 2.1$ Å) is only a secondary minimum on the PES. This time, the lower minimum ($N_{1t}H = 2.2$ Å, $N_{1b}H = 1.0$ Å) corresponds to $[Pb-oxo(U)-H)]^+$ (where N_{1t} has been deprotonated) hydrogen bonded with $[hydroxo(U)H)]^+$ (where N_{1b} has been protonated). The proton transfer from the oxo to the hydroxo tautomer is found to be exothermic ($\Delta\epsilon^{N_{1t}H=1.0\rightarrow2.1}_{N_{1b}H=2.2\rightarrow1.0} = -6$ kcal mol^{-1}). Because of the position of lead connected to O_7, the $[Pb-oxo(U)-H)]^+\cdots[hydroxo(U)H)]^+$ dimer cannot be further stabilized by a relative rotation of the two cycles, contrary to the previous case without lead. As a consequence, no minimum is found in the region of concomitant large $N_{1b}H$ and large $N_{1t}H$. More generally, lead connected to O_7 is expected to generate steric repulsions on the whole PES, and it is worth noting that, even in this unfavorable case, the presence of lead can reverse the energy balance of the proton transfer in a favorable way.

The situation where lead is bonded to O_8 is presented at the bottom of Figure 15. Similar to the case where lead was ligated to O_7, the lower minimum corresponds to $[Pb-oxo(U)-H]^+$ hydrogen bonded to $[hydroxo(U)H)]^+$ ($N_{1t}H = 2.3$ Å, $N_{1b}H = 1.0$ Å). A secondary minimum is attributed to $[Pb-oxo(U)]^{2+}$ hydrogen bonded to [hydroxo(U)] ($N_{1t}H = 1.1$ Å, $N_{1b}H = 1.7$ Å). Again, the proton transfer from the oxo to the hydroxo tautomer is found to be exothermic ($\Delta\epsilon^{N_{1t}H=1.1\rightarrow2.3}_{N_{1b}H=1.7\rightarrow1.0} = -11$ kcal mol^{-1}). Moreover, due to the position of lead (connected to O_8), rotation of the two cycles is allowed again, resulting in a third minimum on the PES ($N_{1t}H = 2.4$ Å, $N_{1b}\cdots H = 2.4$ Å), lying $\Delta\epsilon^{N_{1t}H=2.3\rightarrow2.5}_{N_{1b}H=1.0\rightarrow2.5} = 22$ kcal mol^{-1} above the secondary minimum. This latter well, already observed in the absence of lead (Figure 15, top left), is found to be lower in energy in the present case ($\Delta\epsilon^{N_{1t}H=1.7\rightarrow2.4}_{N_{1b}H=1.0\rightarrow2.4} = -9$ kcal). Note, however, that when lead is connected to O_8, the third minimum corresponds to a region where several states are close in energy. Hence, a multireference treatment is expected to lower that energy well significantly.

Overall, these PES show that the more energetically favorable conformations are $[Pb-(oxo)(U)-H]^+$ H-bonded to $[hydroxo-(U)H)]^+$. Therefore, they support the assumption that the $[Pb-oxo(U)-hydroxo(U)]^{2+}$ complex may dissociate into $[Pb-(oxo)(U)-H]^+ + [hydroxo(U)H)]^+$. Moreover, the proton transfer from oxo(U) to the hydroxo(U) is fast and exothermic. Thus, this reaction scheme or a similar one might participate in the formation of the species observed in our ESIMS and MS/MS experiments. However, further investigations are required to conclude definitely, as several alternative processes (double proton transfers, $N_1 \rightarrow N_3$ proton transfers, non-coplanar uracils, etc.) are also likely to come into play.

4. Conclusion

In the present work, we have attempted to shed some light on proton-transfer processes in lead(II)−uracil systems using geometry optimization calculations. We have investigated uracil 1,3-intramolecular proton transfer as well as uracil−uracil intermolecular proton-transfer processes, the first case being separated into intramolecular events that may or may not require the help of a proton acceptor molecule (namely H_2O and OH^-).

In unimolecular schemes, the proton was transferred from a nitrogen to a neighboring carbonyl oxygen, and we have shown that divalent ions such as Pb^{2+} or $[Pb(H_2O)]^{2+}$ bound to uracil could make the proton-transfer balance exergonic ($\Delta G < 0$), whereas it was always found to be endergonic ($\Delta G > 0$) without the metal. Thus $[Pb(U)]^{2+}$ and $[Pb(H_2O)(U)]^{2+}$ complexes where uracil adopts one of its tautomeric enolic forms are energetically more stable than complexes where uracil adopts its oxo form. Though thermodynamically spontaneous, these processes are kinetically unfavorable and should occur at "geological" time scales. Moreover, it is remarkable that singly charged ions such as $[Pb(OH)]^+$ bound to uracil do not reverse the endergonic proton-transfer balance.

With an additional proton acceptor such as H_2O or OH^- or another uracil, the activation barrier is lowered, making proton transfers both thermodynamically and kinetically favorable. Finally, it is worth noting that, for the intermolecular proton transfer between uracil and H_2O, or uracil and OH^-, or between two uracils, our calculations may acount for the formation of $[Pb(U)-H]^+$ observed in our ESIMS and MS/MS experiments. Moreover, our calculations on the intermolecular proton transfer between two uracils may acount for the simultaneous formation of $[Pb(U)-H]^+$ and $[UH]^+$ ions, as observed in our experiments. Intermolecular proton-transfer mechanisms presented here were based on working hypotheses (i.e., on the relative positions of H_2O and Pb(II) in $[Pb(U)(H_2O)]^{2+}$ ions, on $N_1 \rightarrow N_1$ transfer in $[Pb(U)_2]^{2+}$, or on the assumption of oxo(U) and hydroxo(U) in $[Pb(U)_2]^{2+}$). We thus do not pretend to have given an exhaustive view of all proton-transfer mechanisms taking place in lead−uracil ions. We have instead proposed a feasibility study that serves our aim of demonstrating the pivotal role of lead(II) metal binding to the uracil nucleobase in selected proton-transfer events.

Acknowledgments. C.G. acknowledges P. Chaquin for very fruitful discussions on the theory of reactivity and S. Guillaumont for an introduction to the ESI mass spectrometry experiments. P. Chaquin and H. Loirat are acknowledged for a very careful reading of the manuscript. The authors thank the Institut du Développement et des Ressources en Informatique Scientifique (IDRIS, France) and the Centre de Calculs Recherche et Enseignement (CCRE, University P/M Curie-Jussieu, France) for generous access to their computational facilities. M.P.G. acknowledges support from Genopole-France through an ATIGE Action Thématique Incitative de Génopole.

References and Notes

(1) Duckett, D. R.; Murchie, A. I.; Lilley, D. M. *EMBO J.* **1990**, *9*, 583.

(2) Fenton, R. R.; Stephens, F. S.; Vagg, R. S.; Williams, P. A. *Inorg. Chim. Act.* **1995**, *231*, 73.
(3) Wang, J. P.; El-Sayed, M. A. *Photochem. Photobiol.* **2001**, *73*, 564.
(4) Joyce, G. F. *Annu. Rev. Biochem.* **2004**, *73*, 791.
(5) El-Sayed, M. A.; Yang, D. F.; Yoo, S. K.; Zhang, N. *Isr. J. Chem.* **1995**, *35*, 465.
(6) Arnold, A. P.; Stanley, D. M.; Collins, J. G. *FEBS Lett.* **1995**, *289*, 96.
(7) Salpin, J.-Y.; Boutreau, L.; Haldys, V.; Tortajada, J. *Eur. J. Mass Spectrom.* **2001**, *321*, 7.
(8) Salpin, J.-Y.; Tortajada, J. *J. Mass Spectrom.* **2002**, *379*, 37.
(9) Salpin, J.-Y.; Tortajada, J. *J. Phys. Chem. A* **2003**, *107*, 2943.
(10) Rodriguez-Santiago, L.; Noguera, M.; Sodupe, M.; Salpin, J.-Y.; Tortajada, J. *J. Phys. Chem. A* **107**, *2003*, 9865.
(11) Corral, I.; Mo, O.; Yanez, M.; Salpin, J.-Y.; Tortajada, J.; Radom., L. *J. Phys. Chem. A* **2004**, *108*, 10080.
(12) Guillaumont, S.; Tortajada, J.; Salpin, J.-Y.; Lamsabhi, A. M. *Int. J. Mass. Spectrom.* **2005**, *243*, 279.
(13) Sigel, H.; Costa, C. P. D.; Martin, R. B. *Coord. Chem. Rev.* **2001**, *219*, 435.
(14) Lavanant, H.; Hecquet, E.; Hoppilliard, Y. *Int. J. Mass. Spectrom.* **1999**, *185/186/187*, 11.
(15) Rogalewicz, F.; Hoppilliard, Y.; Ohanessian, G. *Int. J. Mass Spectrom.* **2000**, *201*, 307.
(16) Rogalewicz, F.; Hoppilliard, Y.; Ohanessian, G. *Int. J. Mass Spectrom.* **2000**, *204*, 267.
(17) Reiter, A.; Adams, J.; Zhao, H. *J. Am. Chem. Soc.* **1994**, *116*, 7827.
(18) Peschke, M.; Blades, A.; Kebarle, P. *Int. J. Mass. Spectrom.* **1999**, *185/186/187*, 685.
(19) Burford, N.; Eelman, M.; Groom, K. *J. Inorg. Biochem.* **2005**, *99*, 1992.
(20) Loo, J. *Mass. Spectrom. Rev.* **1997**, *16*, 1.
(21) Frisch, M. J.; Trucks, G. W.; Schlegel, H. B.; Scuseria, G. E.; Robb, M. A.; Cheeseman, J. R.; Zakrzewski, V. G.; Montgomery, J. A., Jr.; Stratmann, R. E.; Burant, J. C.; Dapprich, S.; Millam, J. M.; Daniels, A. D.; Kudin, K. N.; Strain, M. C.; Farkas, O.; Tomasi, J.; Barone, V.; Cossi, M.; Cammi, R.; Mennucci, B.; Pomelli, C.; Adamo, C.; Clifford, S.; Ochterski, J.; Petersson, G. A.; Ayala, P. Y.; Cui, Q.; Morokuma, K.; Malick, D. K.; Rabuck, A. D.; Raghavachari, K.; Foresman, J. B.; Cioslowski, J.; Ortiz, J. V.; Stefanov, B. B.; Liu, G.; Liashenko, A.; Piskorz, P.; Komaromi, I.; Gomperts, R.; Martin, R. L.; Fox, D. J.; Keith, T.; Al-Laham, M. A.; Peng, C. Y.; Nanayakkara, A.; Gonzalez, C.; Challacombe, M.; Gill, P. M. W.; Johnson, B. G.; Chen, W.; Wong, M. W.; Andres, J. L.; Head-Gordon, M.; Replogle, E. S.; Pople, J. A. *Gaussian 98*, revision x.x; Gaussian, Inc.: Pittsburgh, PA, 1998.
(22) Küchle, W.; Dolg, M.; Stoll, A.; Preuss, H. *Mol. Phys.* **1991**, *6*, 1945.
(23) Guillaumont, S.; Tortajada, J.; Salpin, J.-Y.; Lamsabhi, A. M. *Int. J. Mass Spectrom.* **2005**, *243*, 279.
(24) Salpin, J. Y.; Tortajada, J.; Alcami, M.; Mo, O.; Yanez, M. *Chem. Phys. Lett.* **2004**, *383*, 561.
(25) Ochterski, J. W. http://www.Gaussian.com/gwhitepap/thermo.htm., 2000.
(26) Eyring, H. *J. Chem. Phys.* **1935**, *3*, 107.
(27) Millefiori, S.; Alparone, A. *Chem. Phys.* **2004**, *303*, 27.
(28) Leszczyński, J. *J. Phys. Chem.* **1992**, *96*, 1649.
(29) Boughton, J. W.; Pulay, P. *J. Phys. Chem.* **1993**, *47*, 49.
(30) Estrin, D. A.; Paglieri, L.; Corongiu, G. *J. Phys. Chem.* **1994**, *98*, 5653.
(31) Kryachko, E. S.; Nguyen, M. T.; Zeegers-Huyskens, T. *J. Phys. Chem. A* **2001**, *105*, 1288.
(32) Hu, X.; Li, H.; Liang, W.; Han, S. *J. Phys. Chem. B* **2005**, *109*, 5935.
(33) Hu, X.; Li, H.; Liang, W.; Han, S. *J. Phys. Chem. B* **2004**, *108*, 12999.
(34) Zhang, R.; Ceulemans, A.; Nguyen, M. *Mol. Phys.* **2005**, *103*, 983.
(35) Gadre, S. R.; Babu, K.; Rendell, A. P. *J. Phys. Chem. A* **2000**, *104*, 8976.
(36) Smets, J.; McCarthy, W. J.; Adamowicz, L. *J. Phys. Chem.* **1996**, *100*, 14655.
(37) Chandra, A. K.; Nguyen, M. T.; Zeegers-Huyskens, T. *J. Phys. Chem. A* **1998**, *102*, 6010.
(38) van Mourik, T.; Price, S. L.; Clary, D. C. *J. Phys. Chem.* **1999**, *103*, 1611.
(39) Gaigeot, M.-P.; Ghomi, M. *J. Phys. Chem. B* **2001**, *105*, 5007.
(40) Hobza, P.; Sponer, J. *Chem. Rev.* **1999**, *99*, 3247.
(41) Hobza, P.; Sponer, J. *J. Chem. Phys. Lett.* **1998**, *288*, 7.
(42) Leininger, M. L.; Nielsen, I. M. B.; Colvin, M. E.; Janssen, C. L. *J. Phys. Chem. A* **2002**, *106*, 3850.